Modeling nucleation and growth of encapsulated nanocrystals: Kinetic Monte Carlo simulations and rate theory

D. O. Yi,[1] M. H. Jhon,[2,3] I. D. Sharp,[2,3] Q. Xu,[2,3] C. W. Yuan,[2,3] C. Y. Liao,[2,3] J. W. Ager III,[2] E. E. Haller,[2,3] and D. C. Chrzan[2,3]

[1]*Lawrence Livermore National Laboratory, Livermore, California 94550, USA*

[2]*Materials Sciences Division, Lawrence Berkeley National Laboratory, Berkeley, California 94720, USA*

[3]*Department of Materials Science and Engineering, University of California–Berkeley, Berkeley, California 94720, USA*

(Received 10 August 2006; revised manuscript received 19 November 2008; published 12 December 2008)

The nucleation, growth, and early coarsening stages of three-dimensional (3D) cluster growth are modeled with an off-lattice 3D Kinetic Monte Carlo simulation and using a mean-field self-consistent solution to a set of coupled rate equations describing the process. The two approaches yield solutions that agree remarkably well, both for average properties and for the full cluster size distribution throughout the entire growth and coarsening regime. The asymptotic scaling properties of the island size distribution are shown to be similar to those expected from the analysis of Marqusee and Ross.

DOI: 10.1103/PhysRevB.78.245415 PACS number(s): 61.46.Hk, 61.72.up, 81.10.Aj, 81.10.Jt

I. INTRODUCTION

Interest in the fabrication of nanocrystals has grown with their promise as building blocks for novel technical applications in optoelectronic devices,[1–3] chemical sensors and markers,[4–6] and as single-electron memory devices.[7–9] Consequently, nanocrystals have been fabricated via a number of different techniques including wet chemistry[10–12] and cosputtering.[13,14]

Recently, it has been demonstrated that nanocrystals may be fabricated using ion-beam synthesis (IBS).[15–17] In this technique, energetic ions are implanted into a matrix. The ion/matrix combination is chosen to ensure a strong segregating tendency for the implanted species. Subsequent annealing leads to the formation of nanocrystals embedded within the matrix. This processing approach is technologically appealing, as ion implantation is already a commonly applied semiconductor processing route. However, IBS presently lacks the size control believed necessary for many of the mentioned applications. Toward this end, quantitative and accurate models of the nucleation, growth, and coarsening of nanocrystals via IBS are desirable. (Here, the nucleation regime is considered to be the times over which the number density of nanoclusters is increasing. During the growth regime, the number of nanoclusters stays relatively constant. Finally, during the coarsening regime, the number of nanoclusters is decreasing with time.)

In prior work, kinetic Monte Carlo (KMC) studies have been used to understand the growth of implanted materials[16,18] and have shown how experimental parameters can influence the resulting size distribution. Continuum models have also been formulated to describe Ostwald ripening where particle growth occurs at the expense of the dissolution of smaller precipitates.[18–22] Growth of epitaxial thin films has been modeled successfully with a mean-field rate equation theory with reversible[23] and irreversible[24] island growth. Recently an analogous three-dimensional (3D) rate equation theory with irreversible attachment was studied.[25] These two-dimensional (2D) and 3D models describe systems that are driven with a constant flux of atoms, and are in this way different from the nondriven three-dimensional system modeled here. Here, a mean-field formulation is used to describe a nondriven system with reversible attachment.

Under typical IBS conditions, the final cluster size distribution is determined by the conditions during implantation *and* during the subsequent anneal. In this paper, however, we focus on the effects of the post-implantation anneal. The starting point for the analysis is taken to be a spatially random distribution of atoms. Consequently, the final cluster size distributions obtained differ from those observed experimentally for IBS. However, the coarsening dynamics obtained from a self-consistent mean-field treatment neglecting spatial correlations agrees *quantitatively* with the results of KMC simulations for the same problem. It is suggested, therefore, that the time evolution of differing initial seed distributions will also be modeled well, making the tool suitable for modeling the annealing stages associated with IBS.

The following sections describe KMC simulations (Sec. II), the formulation of and solution to the rate equations (Sec. III), the scaling properties of the presented solutions (Sec. IV), and the conclusions.

II. KINETIC MONTE CARLO SIMULATIONS

Nucleation, growth, and coarsening of the embedded species are simulated using a three-dimensional off-lattice KMC algorithm. The simulation cell containing the atoms is assumed to be a cube, and periodic boundary conditions are applied. The cell is chosen to be large enough so that the effects of finite size are negligible; that is, the box length is chosen to be much larger than the distance over which monomers typically travel before being captured. In the simulations presented here, this distance never exceeds 6 nm. Therefore, the typical cell size ranges from 10 to 20 nm on edge. The initial conditions of the simulation box mimic typical experimental conditions.[26] The box contains a fixed number of atoms, distributed randomly. These atoms are the only mobile species in the simulation, and their allowed dynamic processes determine the evolution of the system.

Specifically, only single atoms (monomers) are allowed to migrate through the space. Monomers migrate by hopping a fixed distance a in random directions. A unit vector $\hat{\rho}$ distributed uniformly over the unit sphere is chosen at random, and the new position of the atom is given by $\vec{r}' = \vec{r} + a\hat{\rho}$, with $a = 1$ Å. These random hopping events occur at a rate

$$\nu_{\text{migration}} = \frac{6D}{a^2}, \tag{1}$$

where D is the diffusivity of the monomer in the matrix.

As a monomer makes its way through the matrix, it eventually meets another monomer or cluster and forms a bond. It is assumed that attachment occurs whenever the distance between particles is within a capture distance r_{cap}, measured from the surface of the cluster to the center of the monomer. Every time a monomer hops to a new location, the distances to all particles are checked. Any monomer found within r_{cap} of another particle (monomer or cluster) will be absorbed by the particle and the grown particle moved to a new location, a size-weighted midpoint between the centers of the particles before clustering. The clusters are assumed to relax immediately into a spherical shape. The grown cluster will continue absorbing particles within r_{cap} of its surface until all clusters or monomers within capture distance are absorbed. Moving the grown particles to a new location causes clusters of all sizes to execute a random walk every time they absorb a monomer, the amplitude of their motion decreasing, as the clusters grow larger. Clusters within a distance r_{cap} of each other will coalesce, the new location at a size-weighted midpoint of the original cluster locations.

The dissolution of atoms from a cluster is also included. All atoms on the surface of a cluster are assumed to have equal probability of detachment. Once an atom detaches, it moves to a random location a distance r_{cap} away from the surface of the cluster. The location of the smaller cluster and monomer will be a weighted distance from the location of the original cluster, and again, the cluster performs a random walk. Distances between the detached atom and all other particles are checked. The detachment events, for a cluster with s atoms, occur at a rate

$$\omega_s = 4\pi R_s^2 \frac{D}{a} n_\infty e^{\Gamma/R_s}, \tag{2}$$

where the Gibbs-Thomson relation for the number of atoms in equilibrium with a curved interface of radius R_s is used:[23] $n_1(R_s) = n_\infty \exp(\Gamma/R_s)$. The solubility n_∞ is defined as $n_\infty = n_0 e^{\epsilon_0 \Omega / k_B T}$, where n_0 is the density of sites (albeit in an amorphous matrix,), ϵ_0 is the free-energy change associated with taking a single atom from the matrix and placing it in the cluster, Ω is the atomic volume of the segregating species, k_B is Boltzmann constant, and T is the absolute temperature. The capillary length, $\Gamma = \frac{2\gamma\Omega}{k_B T}$, is directly proportional to the cluster/matrix interface energy, γ. A cluster with s atoms is assumed to be spherical with

$$R_s = \left(\frac{3\Omega}{4\pi} s \right)^{1/3}. \tag{3}$$

Given the rates of allowed processes, KMC simulations then proceed in the standard fashion.[24,27] Specifically, the rates for all allowed processes are summed to create a total rate. A random time consistent with a Poisson process governed by this total rate is generated, and the specific event that occurs at this time is chosen at random from those available, weighing the selection probabilities of the individual events by their rates. After the process is executed, rates are recomputed, and the process is repeated. This procedure obeys detailed balance, and provides an efficient means to study the dynamic evolution of the system. A typical simulation executes 500 million steps, and the presented results are obtained by averaging over nine independent simulations.

III. RATE THEORY

Nucleation, growth, and coarsening processes can also be described by a set of coupled rate equations. Specifically, these equations describe the evolution of the number density of clusters containing s atoms at time t: $\langle n_s(t) \rangle$. Rate equations reflecting the kinetic processes described above appear as

$$\frac{d\langle n_1 \rangle}{dt} = -2D\sigma_1 \langle n_1 \rangle^2 - D \sum_{j \geq 2} \sigma_j \langle n_j \rangle \langle n_1 \rangle + 2\frac{\langle n_2 \rangle}{\tau_2} + \sum_{j \geq 3} \frac{\langle n_j \rangle}{\tau_j}, \tag{4}$$

$$\frac{d\langle n_s \rangle}{dt} = D\sigma_{s-1} \langle n_{s-1} \rangle \langle n_1 \rangle - D\sigma_s \langle n_s \rangle \langle n_1 \rangle - \frac{\langle n_s \rangle}{\tau_s} + \frac{\langle n_{s+1} \rangle}{\tau_{s+1}}, \tag{5}$$

with $s \geq 2$.

The terms in these equations are straightforward. Clusters are assumed to grow and shrink through the attachment and detachment of monomers. The capture length for a cluster of s atoms is given by σ_s, and the first two terms on the right-hand side in Eq. (5) reflect these processes. The final two terms in Eq. (5) account for the effects of detachment processes on the cluster number densities. Equation (4) governs the evolution of the number density of monomers. Monomers are annihilated by their attachment to other monomers [first term on the right-hand side of Eq. (4)] or attachment to existing clusters [second term on the right-hand side of Eq. (4)]. Similarly, monomers are created when atoms detach from existing clusters [last two terms on the right-hand side of Eq. (4)].

In order to solve Eqs. (4) and (5), accurate descriptions of the reaction rates, the capture lengths σ_s, and escape rates, $1/\tau_s$, are needed. Bales and Chrzan[24] used a self-consistent mean-field formulation in 2D to derive expressions for the 2D equivalent of the capture lengths. Later, Bales and Zangwill[23] extended the theory to allow atom detachment, deriving an expression for the capture length and escape rate. A similar derivation follows in 3D.

The rate equations describe average quantities and do not specify the capture lengths nor escape rates. One could include spatial dependencies for each monomer and cluster

species, but this would mean solving partial differential equations with variables in both time and space, in very complicated geometries. For this reason, a mean-field approach is used, in which a monomer field density given by $n_1(\vec{r},t)$ interacts with average atomic and cluster densities $\{\langle n_1\rangle,\langle n_2\rangle,\ldots,\langle n_s\rangle\}$. The escape rate and capture lengths are then derived self-consistently by applying the proper boundary conditions and ensuring atomistic reactions at the boundaries are specified in the continuum.

Consider a cluster with radius R_s embedded in a monomer field density $n_1(\vec{r},t)$. The monomer field is described everywhere in space and time according to the diffusion-reaction equation,

$$\frac{\partial n_1(\vec{r},t)}{\partial t} = D\nabla^2 n_1(\vec{r},t) + \mathcal{J} - D\xi^{-2} n_1(\vec{r},t). \tag{6}$$

If the monomer field is assumed to interact with average monomer and cluster densities, these interaction strengths are encompassed in D, $\mathcal{J}$, and ξ, where D is the diffusion of monomers in the matrix, $\mathcal{J}$ is the flux of monomers that have escaped from other clusters, and ξ is the typical distance a monomer travels before being captured by a cluster or another monomer. $\mathcal{J}$ and ξ are calculated from the self-consistent condition,

$$\lim_{\vec{r}\to\infty} n_1(\vec{r},t) = \langle n_1(t)\rangle, \tag{7}$$

and the following associations are made [comparing Eq. (6) to Eq. (4)]:

$$\mathcal{J} = 2\frac{\langle n_2\rangle}{\tau_2} + \sum_{j\geq 3}\frac{\langle n_j\rangle}{\tau_j}, \tag{8}$$

$$\xi^{-2} = 2\sigma_1\langle n_1\rangle + \sum_{s\geq 2}\sigma_s\langle n_s\rangle. \tag{9}$$

Then, subtracting Eq. (4) from Eq. (6), and assuming that as time evolves, the change in $n_1(\vec{r},t)$ does not vary far from the change in its average value, $\langle n_1\rangle$ yields

$$0 \approx \frac{\partial n_1}{\partial t} - \frac{d\langle n_1\rangle}{dt} = D\nabla^2 n_1 - D\xi^{-2}\{n_1 - \langle n_1\rangle\}. \tag{10}$$

The Helmholtz equation [Eq. (10)] can be solved in 3D subject to the boundary condition for the monomer density at infinity, Eq. (7), and a condition for the monomer flux at the boundary of the cluster,

$$n_1(r) = -Ak_0\left(\frac{r}{\xi}\right) + \langle n_1\rangle, \tag{11}$$

where A is a constant defined by boundary conditions. The spherical Bessel function k_0 is given by

$$k_0(x) = \frac{e^{-x}}{x}. \tag{12}$$

In the KMC simulations, r_{cap} is defined to be the distance between particle surface and atom center before attachment or after detachment. In the same way, atoms a distance r_{cap} away are considered as atoms ready to attach to the cluster. Within r_{cap}, there is a difference in energy barriers to attachment and detachment that leads to a difference in the rates of transition. Because there is a difference in forward and backward rates, the diffusion-reaction equation [Eq. (6)] (with constant diffusivity) is not valid in this region.[28,29] Therefore, its solution given by Eq. (11) is valid only for $r \geq R_s + r_{\text{cap}}$.

A proper definition of the boundary conditions will involve matching the outgoing flux of monomers given by the continuum description to its atomistic description. The continuum flux, given by Fick's law, is valid only for $r \geq R_s + r_{\text{cap}}$. The atomistic flux of incoming particles is proportional to the number of atoms at $r = R_s + r_{\text{cap}}$, and it is assumed that they are all ready for attachment (all atoms have crossed over the barrier to attachment). The flux of atoms leaving the cluster is evaluated at $r = R_{s+1}$ since atoms leaving a cluster with s atoms necessarily detach from a cluster of size $s+1$.

Solving for the continuum description of the monomer density for $r \geq R_s + r_{\text{cap}}$, Eq. (11) becomes

$$n_1(r) = \langle n_1\rangle - [\langle n_1\rangle - n_1(R_s + r_{\text{cap}})] \times \frac{R_s + r_{\text{cap}}}{r}\exp\left(\frac{-r + R_s + r_{\text{cap}}}{\xi}\right). \tag{13}$$

The total outgoing continuum flux at $r = R_s + r_{\text{cap}}$ is then given by

$$\begin{aligned} J_{\text{continuum}} &= -4\pi(R_s + r_{\text{cap}})^2 D\left.\frac{dn_1}{dr}\right|_{R_s + r_{\text{cap}}} \\ &= -4\pi(R_s + r_{\text{cap}})^2 D[\langle n_1\rangle - n_1(R_s + r_{\text{cap}})] \times\left(\frac{1}{\xi} + \frac{1}{R_s + r_{\text{cap}}}\right). \end{aligned} \tag{14}$$

The number of monomers at $R_s + r_{\text{cap}}$ is not known, but one can use the atomistic total flux to find it,

$$\begin{aligned} J_{\text{atomistic}} &= J_{\text{detach}} - J_{\text{attach}} \\ &= \omega_{s+1} - 4\pi(R_s + r_{\text{cap}})^2\frac{D}{a}n_1(R_s + r_{\text{cap}}). \end{aligned} \tag{15}$$

The total flux of atoms detaching from clusters with $s+1$ atoms is just given by the rate of detachment, ω_{s+1} [defined in Eq. (2)]. The total flux of atoms attaching to clusters with s atoms depends on the number of atoms at $R_s + r_{\text{cap}}$. Equating atomistic [Eq. (15)] to continuum [Eq. (14)] descriptions of the total flux allows one to solve for $n_1(R_s + r_{\text{cap}})$. Then substituting this into Eq. (15) yields

$$J_{\text{atomistic}} = 4\pi(R_s + r_{\text{cap}})^2\left[\frac{a\omega_{s+1}}{4\pi(R_s + r_{\text{cap}})^2} - D\langle n_1\rangle\right] \times \frac{R_s + r_{\text{cap}} + \xi}{a(R_s + r_{\text{cap}} + \xi) + \xi(R_s + r_{\text{cap}})}. \tag{16}$$

This describes the total outgoing rate of monomers and can be equated to the outgoing rate of $\langle n_1\rangle$ as given by the mean-field model [Eq. (4)]. The first term in Eq. (16) describes the rate of escape from a cluster with $s+1$ atoms, $1/\tau_{s+1}$, while the second term describes the rate of attachment to clusters of size s, $D\sigma_s\langle n_1\rangle$. The reaction rates are then given by

$$\sigma_s = 4\pi(R_s + r_{\text{cap}})^2 \frac{R_s + r_{\text{cap}} + \xi}{a(R_s + r_{\text{cap}} + \xi) + \xi(R_s + r_{\text{cap}})}, \quad (17)$$

$$\frac{1}{\tau_s} = \frac{a\sigma_{s-1}\omega_s}{4\pi(R_{s-1} + r_{\text{cap}})^2} = \sigma_{s-1}\left(\frac{R_s}{R_{s-1} + r_{\text{cap}}}\right)^2 Dn_\infty \exp(\Gamma/R_s), \quad (18)$$

where the last equality in Eq. (18) uses Eq. (2) for the detachment rate. It should be noted that Eq. (17) reproduces the capture number for irreversible growth in 3D derived by Shi *et al.*[25] if one takes $r_{\text{cap}}=0$ and $a=0$.

Both the capture length and the escape rate are nonlinear functions of the cluster radius and ξ. Note that ξ is also a function of all the capture lengths and particle densities [see Eq. (9)]. As time evolves, monomer densities decrease while cluster densities increase. This results in an increase in the distance monomers must travel before capture. Larger clusters are more efficient at capturing monomers, as given by Eq. (17), and less prone to losing monomers, as given by Eq. (18). Thus, the equations allow for coarsening.

In order to compare the rate equation formulation to KMC simulations, one must ensure that parameters used in one model are the same as those used in the simulation. The parameters that are key to the comparability of rate equations to KMC are the diffusivity of the monomer in the matrix D, the hop distance a, the capture distance r_{cap}, the initial monomer concentration n_0, the monomer solubility n_∞, and the capillary length Γ.

In the following plots, unless stated otherwise, we measure all lengths in terms of the hop distance a which is taken to be 1 Å. Dimensionless quantities are indicated by a tilde. For example, the dimensionless number density of islands $\langle\tilde{N}\rangle$ is defined according to $\langle\tilde{N}\rangle = a^3\langle N\rangle$. All times are measured in units of a^2/D, with D the diffusivity. Accordingly, $\tilde{t} \equiv Dt/a^2$. As long as the same diffusivity is used in the rate equations and KMC, the time scale will be properly defined. We have set $D=1$ Å^2/sec. The capture distance r_{cap} is set to 1 Å, and determines the interaction distance between particles. The initial monomer concentration determines the number of clusters in the system, as will be seen shortly. The expression for the detachment rate shown in Eq. (2) must be the same for both the rate equation formulation and KMC simulation.

Figure 1 plots the predictions of the continuum rate equation formulation and KMC simulations for both the average monomer density and the average number density of clusters, $\langle\tilde{N}\rangle$,

$$\langle\tilde{N}\rangle = \sum_{s=2}^{\infty} \langle\tilde{n}_s\rangle, \quad (19)$$

for typical growth conditions. While the agreement between the two theories is overall quite good, there is noticeable disagreement in both the nucleation and coarsening stages of evolution. Specifically, the rate equation theory underestimates the nucleation rate, as evidenced by an excess of monomers and sparsity of clusters in the nucleation stages (i.e., $\tilde{t} < 10^{-2}$) of the rate equation solution as compared with

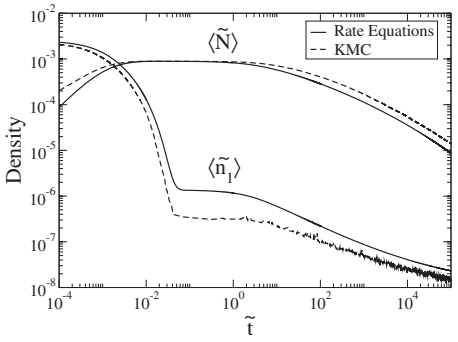

FIG. 1. Evolution of monomer and cluster density for $n_0 = 0.0025$ Å^{-3}, $n_\infty = 10^{-8}$ Å^{-3}, and $\Gamma = 5$ Å.

KMC simulation results. Further, the rate equation theory overestimates the desorption rate of monomers from existing clusters, as evidenced by the reduced number of clusters during the coarsening stages (i.e., $\tilde{t} > 1$) in the rate equation results as compared with KMC results. Both of these discrepancies must stem from the mean field and/or the adiabatic hypothesis [Eq. (10)].

In the present situation, the nucleation rate is controlled by r_{cap} and the desorption rate scales with n_∞. Both of the shortcomings within the mean-field theory predictions can be corrected by using r_{cap} and n_∞ as one-time adjustable parameters. Specifically, choosing

$$r_{\text{cap}}^{\text{RE}} = 1.61 r_{\text{cap}}^{\text{KMC}} \quad (20)$$

ensures that the nucleation stage of the growth process is modeled accurately, and choosing

$$n_\infty^{\text{RE}} = 0.59 n_\infty^{\text{KMC}} \quad (21)$$

ensures that the coarsening behavior is modeled properly, irrespective of growth conditions. Upon enforcing Eqs. (20) and (21) the resulting agreement between KMC and rate equation approaches is then nearly perfect (here the superscripts KMC and RE refer to KMC and rate equation formulations, respectively). To establish this point, results are presented for varying values of key parameters: initial monomer concentration (Fig. 2), solubility (Figs. 3 and 4), and capillary length (Fig. 5). In all cases, KMC results are nearly indistinguishable from the predictions of rate equations. From here on, Eqs. (20) and (21) are assumed to hold.

The solutions display additional scaling behaviors. Varying the initial monomer density affects the nucleation regime only (see Fig. 2). The curves for $\langle\tilde{n}_1\rangle$, $\bar{s}$, and $\langle\tilde{N}\rangle/\tilde{n}_0$ are equivalent (coincide) in the coarsening regime ($\langle\tilde{N}\rangle/\tilde{n}_0 \sim 1/\bar{s}$). Nucleation occurs earlier for larger n_0. Because the decrease in monomer density is proportional to n_0^2,

$$\frac{d\langle n_1\rangle}{dt} \sim \langle n_1\rangle^2 \sim n_0^2, \quad (22)$$

the time it takes to nearly deplete all monomers during cluster formation is inversely proportional to n_0. Therefore, a high monomer concentration results in a shorter time spent in the nucleation regime.

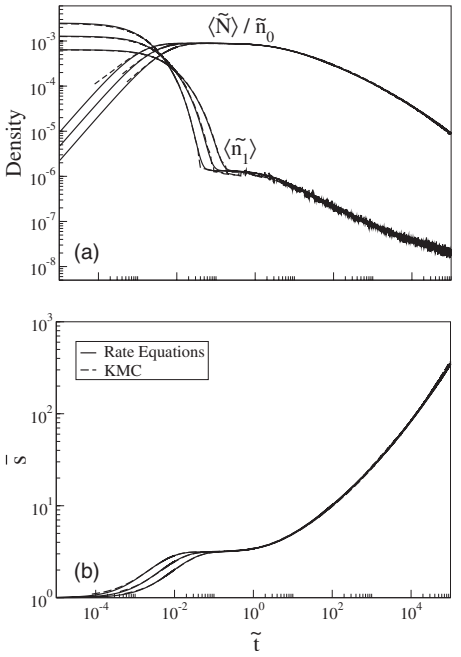

FIG. 2. (a) Evolution of monomer and cluster density and (b) average cluster size for varying n_0. The initial concentration varies as n_0=0.0025, 0.00128, 0.00064 Å^{-3} from left to right for $\langle\tilde{N}\rangle/\tilde{n}_0$ and $\bar{s}$ and from top to bottom in the far left of the plot for $\langle\tilde{n}_1\rangle$. Other parameters are $n_\infty^{\mathrm{RE}}=10^{-8}$ Å^{-3} and $\Gamma=5$ Å.

To establish this point, in Fig. 3, the monomer and cluster densities and average cluster sizes are plotted against $\tilde{t}\tilde{n}_\infty^{2/3}$ for varying solubility, and one notices that doing so affects the coarsening regime only. As the figure shows, decreasing

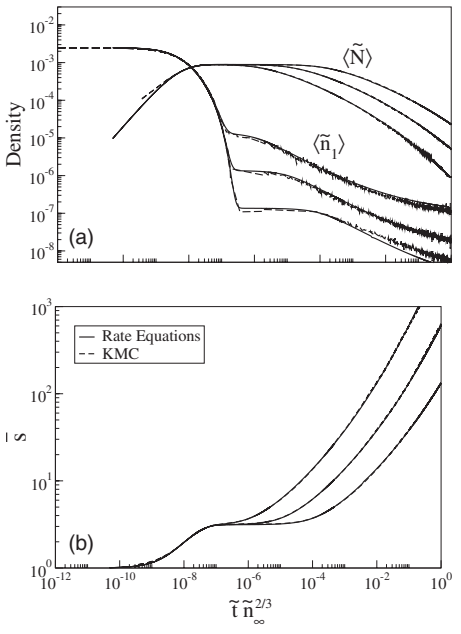

FIG. 3. (a) Evolution of monomer and cluster density and (b) average cluster size for varying n_∞ for n_0=0.0025 Å^{-3} and Γ =5 Å plotted as a function of $\tilde{t}\tilde{n}_\infty^{2/3}$. The solubility varies as n_∞^{RE} $=10^{-7},10^{-8},10^{-9}$ Å^{-3} from left to right for $\langle\tilde{N}\rangle$ and $\bar{s}$ and from top to bottom for $\langle\tilde{n}_1\rangle$.

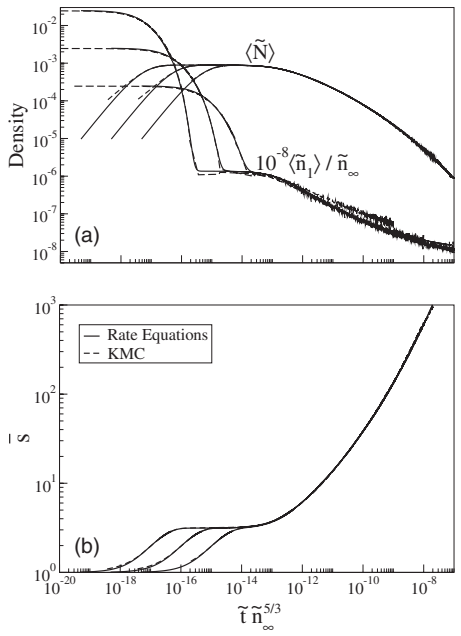

FIG. 4. (a) Evolution of monomer and cluster density and (b) average cluster size for varying n_∞ for n_0=0.0025 Å^{-3}, Γ=5 Å. $\langle\tilde{n}_1\rangle$ is scaled by $10^{-8}/\tilde{n}_\infty^i$. (The factor of 10^{-8} ensures the plots for $\langle\tilde{n}_1\rangle$ are within the plotted range.) The solubility varies as n_∞^{RE} $=10^{-7},10^{-8},10^{-9}$ Å^{-3} from right to left for $\langle\tilde{N}\rangle$ and $\bar{s}$ and from bottom to top for $\langle\tilde{n}_1\rangle$.

the solubility decreases the number of monomers in equilibrium with the cluster interface, decreasing the rate of coarsening. Equation (18) further states that the time it takes an atom to escape a cluster is inversely proportional to

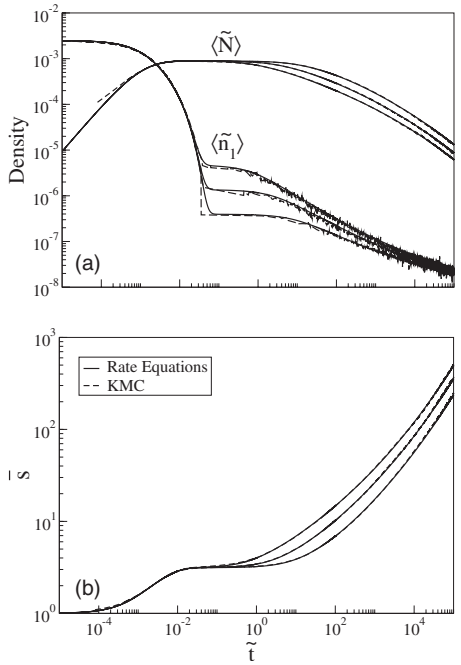

FIG. 5. (a) Evolution of monomer and cluster density and (b) average cluster size for varying Γ for n_0=0.0025 Å^{-3} and n_∞^{RE} $=10^{-8}$ Å^{-3}. The capillary length varies as $\Gamma=4,5,6$ Å from top to bottom for $\langle\tilde{N}\rangle$ and from bottom to top for $\langle\tilde{n}_1\rangle$ and $\bar{s}$.

$n_\infty \exp(\Gamma/R_s)$. So the lower the solubility n_∞, the longer an atom will want to stay attached to a cluster. Monomer concentration also behaves as $1/\tau_s$ [see Eq. (4)] in the coarsening regime and, therefore, scales with n_∞. Figure 4 shows that if one plots $\bar{s}$, $\langle\tilde{N}\rangle/\langle\tilde{n}_o\rangle$, and $\langle\tilde{n}_1\rangle$ versus $\tilde{t}\tilde{n}_\infty^{5/3}$ the solutions to varying solubility are equivalent in the coarsening regime.

Finally, in Fig. 5, the monomer and cluster densities and average cluster sizes are plotted against time for varying capillary length, and again, only the coarsening regime is affected. Varying the capillary length results in a nonlinear dependence in the coarsening regime. The rate of coarsening is proportional to $n_\infty \exp(\Gamma/R_s)$, as previously discussed. A larger Γ results in a shorter escape time and increase in monomers outside a cluster interface and, thus, increases the rate of coarsening. Additionally, the nonlinear dependence on the cluster radius is noted in the difference between the curves in the early and later coarsening stages. When coarsening begins, cluster radii are on average small, and $\exp(\Gamma/R_s)$ is large. As coarsening continues, the clusters grow and finally $\exp(\Gamma/R_s) \to 1$. This indicates that for systems with very large clusters, a change in interfacial energy (or capillary length) will not affect the rate of coarsening.

IV. SCALING THEORY

Scaling theories have been used to analyze many different systems with seemingly intractable complexity by identifying physical similarities in the system at different time and/or length scales. The use of scaling theories spans many decades in particle physics and condensed-matter theory, and has covered systems exhibiting equilibrium critical behavior, percolating systems, and dynamically driven systems. In particular, scaling arguments were used to analyze 2D epitaxial growth to show the existence of scaled distribution functions.[24,25,30] Identical scaling arguments work here as well, and the scaling function takes the same form.

In the asymptotic limit of large cluster size, it is assumed that the only important size is given by average cluster size $\bar{s}$. The cluster size distribution function is defined in terms of the cluster size s and the average cluster density,[24,31,32]

$$f(s,t) = f[s,\bar{s}(t)] = \frac{s\langle n_s(t)\rangle}{n_0}. \tag{23}$$

The scaling hypothesis declares that the distribution function satisfies the homogeneity condition,

$$f[\gamma s, \gamma\bar{s}(t)] = \gamma^{-\theta} f[s,\bar{s}(t)]. \tag{24}$$

If $\gamma = \bar{s}(t)^{-1}$ is chosen, the distribution function can be rewritten in terms of a scaling function g,

$$f[s,\bar{s}(t)] = \bar{s}(t)^{-\theta} g[s/\bar{s}(t)]. \tag{25}$$

To find the exponential θ, conservation of particle number is employed to derive

$$1 = \bar{s}^{1-\theta} \int_0^\infty g(s/\bar{s}) d(s/\bar{s}). \tag{26}$$

The solution to this equation requires that $\theta = 1$. Thus, the scaling function is

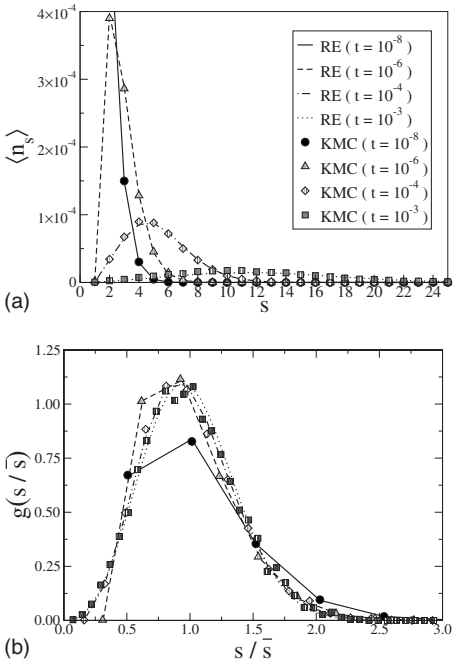

FIG. 6. (a) Unscaled and (b) scaled size distributions shown for the growth and coarsening regimes for KMC and rate equation solutions.

$$g(s/\bar{s}) = \bar{s}\frac{s\langle n_s(t)\rangle}{n_0}. \tag{27}$$

It is assumed that this scaled form of the distribution function holds true. By plotting $g(s/\bar{s})$ versus $s/\bar{s}(t)$ at several values of t, the scalability of the distribution function for the system can be determined. The nucleation regime does not scale since the scaling form is only valid in the coarsening regime. And actually, the system is not fully in the asymptotic limit of large $\bar{s}$ where scaling is valid. In fact, even at the end of the simulation, the asymptotic regime is not yet reached. Figure 6 also shows that, in striking contrast to the driven 2D mean-field solution, the 3D nondriven mean-field solution gives a quantitatively accurate description of the evolving cluster size distribution. Thus the rate equations can be used directly in further detailed analyses.

In the asymptotic long-time limit, the rate equation formulation can be compared to classical diffusion-limited coarsening theories. A self-similar state is assumed to exist. Taking the continuum limit of Eq. (5),

$$\frac{d\langle n(s)\rangle}{dt} + \frac{d}{ds}\left[\left(D\langle n_1\rangle\sigma(s) - \frac{1}{\tau(s)}\right)\langle n(s)\rangle\right] = 0. \tag{28}$$

Noting that the average cluster density distribution must obey a continuity equation of the form

$$\frac{d\langle n(s)\rangle}{dt} + \frac{d}{ds}\left(\frac{ds}{dt}\langle n(s)\rangle\right) = 0 \tag{29}$$

allows one to identify the following expression for the rate of change of a particle of size s:

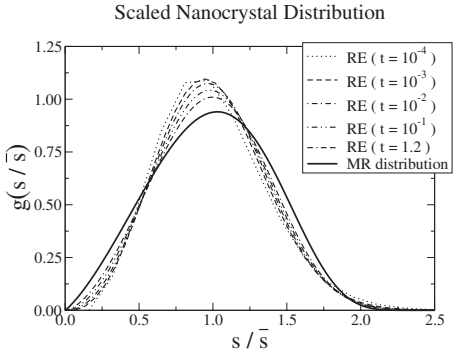

FIG. 7. Rate equation scaled distributions compared with MR prediction for coarsening with $\phi_\infty=0.05$. KMC results are indistinguishable from RE predictions and are not shown for simplicity.

$$\frac{ds}{dt} = D\langle n_1\rangle\sigma(s) - \frac{1}{\tau(s)}. \tag{30}$$

Equation (30) has a simple physical interpretation. The rate at which atoms leave a cluster is simply $1/\tau(s)$, and the rate at which atoms attach to the cluster is given by $D\langle n_1\rangle\sigma(s)$. Keeping only terms of zeroth order in a/ξ and R_{cap}/ξ, the continuum limit of Eq. (17) is

$$\sigma(s) = 4\pi R(s)\frac{R(s)+\xi}{\xi}. \tag{31}$$

Combining Eqs. (30) and (31) with the continuum version of Eq. (18) relating $\tau(s)$ to $\sigma(s)$ yields

$$\frac{dR}{dt} = \frac{D\Omega n_\infty}{R}[\langle n_1\rangle - n_\infty \exp(R/\Gamma)]\left(1+\frac{R}{\xi}\right). \tag{32}$$

An expression for ξ may be found by combining a continuum form of Eq. (9) with Eq. (31),

$$\xi^{-2} = 4\pi\int_0^\infty \frac{R(s)^2}{\xi}\langle n(s)\rangle ds + 4\pi\int_0^\infty R(s)\langle n(s)\rangle ds. \tag{33}$$

By solving Eqs. (29), (32), and (33) self-consistently, the steady-state self-similar distribution may be found. If the second term of Eq. (33) dominates, these equations are identical to those analyzed by Marqusee and Ross (MR) for diffusion-limited coarsening.[33] The effect of the equilibrium volume fraction $\phi_\infty=n_0/\Omega$ is included through the self-consistent condition on ξ. As $\xi\to\infty$, this distribution recovers the classical zero-volume fraction limit, the Lifshitz-Slyosov-Wagner (LSW) theory.[34,35]

V. DISCUSSION

This algebraic analysis suggests that in the asymptotic limit, the rate equation solutions approach the MR solution. Figure 7 compares the numerical solutions of the rate equations [Eq. (27)] to the MR solution in s space. From the plot, it is evident that the numerical solution to the rate equations has not yet converged to a scaled solution. (The apparent differences between scaled distributions stemming from successive times are not yet decreasing rapidly.) We conclude that the numerical solutions (and, hence, KMC simulations) are not yet in the asymptotic scaling regime. Presently, the computational resources available to us preclude integrating for times long enough to reach the asymptotic solution, and we cannot yet reach conclusions concerning the asymptotic properties of the numerical solutions to the rate equations. Similarly, Snyder *et al.*[36] found that relaxation times for transient coarsening were very long.

The present model does not include correlations, unlike other treatments of coarsening.[37] However, the quantitative agreement between the self-consistent mean-field treatment and KMC simulations suggests that if these correlations influence the cluster size distributions, their influence can be mimicked by a rescaling of the equilibrium solubility, n_∞, and the capture radius, r_{cap}, by respective factors that are fixed for all conditions considered. The resulting self-consistent mean-field theory offers substantial simplification over direct simulation including the spatial correlations, and may thus allow more accurate deterministic modeling of larger systems than possible within other approaches.

The computational expense required by the rate equations depends critically on the number of equations to be solved. On a typical state of the art workstation, the solution to problems involving only clusters with fewer than 1000 atoms can be obtained in a day using standard integration schemes. Presently, it is not possible to obtain the solution with maximum cluster sizes comparable to those experimentally observed. It should be noted, however, that the solution need be obtained only once; there is no need to average over multiple configurations. In this respect, the treatment is efficient.

Unfortunately, the model presented here for cluster size distributions does not describe well experimentally obtained cluster size distributions: The theory invariably renders a negatively skewed profile as it approaches the asymptotic solution. In contrast, experimentally observed profiles tend to be broader and approach a logarithm-normal-like shape.[26,38,39] A more complete theory must include the evolution of clusters during the implantation process, as suggested by Heinig and collaborators.[38]

VI. CONCLUSION

The nucleation, growth, and coarsening of nanoclusters embedded in a matrix have been successfully modeled using both atomistic KMC simulations and a mean-field rate equation model. Remarkable agreement between theory and simulation resulted after identifying an understated nucleation rate and an overstated detachment rate within the mean-field theory. Correction of these difficulties within the mean-field formalism leads to a continuum theory that agrees *quantitatively* with results of KMC simulations for a wide variety of initial monomer densities, solubilities, and capillary lengths. Further, the solutions have simple scaling dependencies on $\langle n_1\rangle$ and n_∞. Scaling theory provides a scaling form for the size distributions and allows comparison to the prior prediction for particle coarsening. The evolution of embedded species through the growth stage and coarsening regime appears to approach asymptotically the MR solution.

Numerical solutions of the rate equations, however, are not yet in the asymptotic regime.

The rate theory and KMC model developed, along with the scaling arguments, can be used to predict distributions of nanocrystal sizes. If the path to creating nanoclusters is given by atom-by-atom growth with detachment kinetics, knowledge of experimental parameters would provide a way to predict the size profile of nanocrystals. This assumption, however, is not sufficient to explain experimentally obtained size distributions. The observed profiles tend to be broad and positively skewed (more weighted on the smaller sizes)—a result impossible to attain if one anneals the system starting with a random distribution of atoms. This implies that there are other mechanisms at work during IBS, which seed the annealing stage with a post-implantation size distribution.

ACKNOWLEDGMENTS

The authors acknowledge A. Kubota and W. G. Wolfer for insightful discussions of KMC algorithms and rate theory. D.C.C and E.E.H. acknowledge support from the Miller Institute for Basic Research in Science. This work was supported in part by the Director, Office of Science, Office of Basic Energy Sciences, Division of Materials Science and Engineering of the U.S. Department of Energy under Contract No. DE-AC02-05CH11231 and in part by U.S. NSF under Grant No. DMR-0109844.

[1] X. Duan, Y. Huang, Y. Cui, J. Wang, and C. M. Lieber, Nature (London) **409**, 66 (2001).
[2] Y. Huang, X. Duan, and C. M. Lieber, Small **1**, 142 (2005).
[3] C. Wang, M. Shim, and P. Guyot-Sionnest, Science **291**, 2390 (2001).
[4] A. N. Shipway, E. Katz, and I. Willner, ChemPhysChem **1**, 18 (2000).
[5] Q. Wan, Q. H. Li, Y. J. Chen, T. H. Wang, X. L. He, J. P. Li, and C. L. Lin, Appl. Phys. Lett. **84**, 3654 (2004).
[6] J. Wang, Electroanalysis **17**, 7 (2005).
[7] S. Tiwari, F. Rana, H. Hanafi, A. Harstein, E. Crabbé, and K. Chan, Appl. Phys. Lett. **68**, 1377 (1995).
[8] J. von Borany, T. Gebel, K. H. Stegemann, H. J. Thees, and M. Wittmaack, Solid-State Electron. **46**, 1729 (2002).
[9] Y. Q. Wang *et al.*, Appl. Phys. Lett. **84**, 5407 (2004).
[10] V. F. Puntes, K. M. Krishnan, and A. P. Alivisatos, Science **291**, 2115 (2001).
[11] A. L. Rogach, D. V. Talapin, E. V. Shevchenko, A. Kornowski, M. Haase, and H. Weller, Adv. Funct. Mater. **12**, 653 (2002).
[12] X. Wang, J. Zhuang, Q. Peng, and Y. Li, Nature (London) **437**, 121 (2005).
[13] M. Fujii, S. Hayashi, and K. Yamamoto, Jpn. J. Appl. Phys., Part 1 **30**, 687 (1991).
[14] W. K. Choi, V. Ng, S. P. Ng, H. H. Thio, Z. X. Shen, and W. S. Li, J. Appl. Phys. **86**, 1398 (1999).
[15] C. W. White, J. D. Budai, S. P. Withrow, J. G. Zhu, E. Sonder, R. A. Zuhr, A. Meldrum, D. M. Hembree, Jr., D. O. Henderson, and S. Prawer, Nucl. Instrum. Methods Phys. Res. B **141**, 228 (1998).
[16] M. Strobel, K.-H. Heinig, W. Möller, A. Meldrum, D. S. Zhou, C. W. White, and R. A. Zhur, Nucl. Instrum. Methods Phys. Res. B **147**, 343 (1999).
[17] I. D. Sharp, D. O. Yi, Q. Xu, C. Y. Liao, J. W. Beeman, Z. Liliental-Weber, K. M. Yu, D. Zhakarov, J. W. Ager III, D. C. Chrzan, and E. E. Haller, Appl. Phys. Lett. **86**, 063107 (2005).
[18] M. Strobel, K.-H. Heinig, and W. Möller, Phys. Rev. B **64**, 245422 (2001).
[19] L. Ratke and P. W. Voorhees, *Growth and Coarsening*, 1st ed. (Springer-Verlag, New York, 2002).
[20] N. E. B. Cowern, G. Mannino, P. A. Stolk, F. Roozeboom, H. G. A. Huizing, J. G. M. van Berkum, F. Cristiano, A. Claverie, and M. Jaraíz, Phys. Rev. Lett. **82**, 4460 (1999).
[21] C. Bonafos, B. Colombeau, A. Altibelli, M. Carrada, G. B. Assayag, B. Garrido, M. López, A. Pérez-Rodrígez, J. R. Morante, and A. Claverie, Nucl. Instrum. Methods Phys. Res. B **178**, 17 (2001).
[22] C. Bonafos, B. Colombeau, M. Carrada, A. Altibelli, and A. Claverie, Mater. Sci. Eng., B **88**, 112 (2002).
[23] G. S. Bales and A. Zangwill, Phys. Rev. B **55**, R1973 (1997).
[24] G. S. Bales and D. C. Chrzan, Phys. Rev. B **50**, 6057 (1994).
[25] F. S. Shi, Y. Shim, and J. G. Amar, Phys. Rev. B **71**, 245411 (2005).
[26] I. D. Sharp, Q. Xu, C. Y. Liao, D. O. Yi, J. W. Beeman, Z. Liliental-Weber, K. M. Yu, D. Zhakarov, J. W. Ager III, D. C. Chrzan, and E. E. Haller, J. Appl. Phys. **97**, 124316 (2005).
[27] P. A. Maksym, Semicond. Sci. Technol. **3**, 594 (1988).
[28] W. G. Wolfer (private communication).
[29] M. E. Glicksman, *Diffusion in Solids*, 1st ed. (Wiley, New York, 2000).
[30] M. C. Bartelt and J. W. Evans, Phys. Rev. B **46**, 12675 (1992).
[31] P. Meakin, Rep. Prog. Phys. **55**, 157 (1992).
[32] D. Stauffer and A. Aharony, *Percolation Theory*, 2nd ed. (CRC, Boca Raton, 1994).
[33] J. A. Marqusee and J. Ross, J. Chem. Phys. **80**, 536 (1984).
[34] I. M. Lifshitz and V. V. Slyosov, J. Phys. Chem. Solids **19**, 35 (1961).
[35] C. Wagner, Z. Elektrochem. **65**, 581 (1961).
[36] V. A. Snyder, J. Alkemper, and P. W. Voorhees, Acta Mater. **49**, 699 (2001).
[37] M. Marder, Phys. Rev. Lett. **55**, 2953 (1985).
[38] K. H. Heinig, T. Müller, B. Schmidt, M. Strobel, and W. Möller, Appl. Phys. A **77**, 17 (2003).
[39] P. Dubcek, B. Pivac, I. Capan, S. Bernstorff, R. Mu, and B. Vlahovic, Vacuum **82**, 130 (2007).